Long-term Hot Corrosion Behavior of Boiler Tube Alloys in Waste-to-Energy Plants

Jing Liu, Devy Dyson, Edouard Asselin

Department of Materials Engineering, The University of British Columbia, Vancouver, BC, Canada

This is a post-peer-review, pre-copyedit version of an article published in Oxidation of Metals. The final authenticated version is available online at: http://dx.doi.org/10.1007/s11085-016-9627-y

Abstract

Accelerated corrosion of candidate alloys was induced by metal chlorides/sulfates at 500°C. Results suggest that the corrosivity of the studied metal chlorides increases in the order $CaCl_2$ < NaCl < KCl < $ZnCl_2$ < $PbCl_2$ < $FeCl_2$. Mechanisms to explain the different impacts of chlorides were proposed. It is believed that materials exposed to chloride salts corrode through vicious cycles, in which a shorter path of the cycle leads to a higher corrosion rate. Experimental results confirmed that $FeCl_2$, with the shortest path of the corresponding vicious cycle, resulted in the highest corrosion rate. It is also confirmed that the sulfates of Zn and Pb are less corrosive than their chlorides for the alloys tested. A kinetic study on the hot corrosion of T22, Esshete 1250 and Sanicro 28 was carried out under simulated waste-to-energy (WTE) ashes at 500°C for 1000 h. Results from the kinetic study show that T22, Esshete 1250, and Sanicro 28 exhibited comparable performance for short-term exposure; however, the degradation thickness presented a clear trend after the 1000 h exposures in terms of decreasing resistance to corrosion: T22 > Esshete 1250 > Sanicro 28. EDX maps confirmed the role of Ni/Cr for slowing the corrosion kinetics of these three alloys.

Keywords WTE · Hot corrosion · Candidate alloys · Chlorides · Sulfates

1 Introduction

In recent decades, waste-to-energy (WTE) technology has been increasingly utilized for the disposal of solid wastes, generating energy in the form of electricity and/or heat from their incineration [1–4]. Compared to landfill disposal, combustion can reduce the environmental burden of disposing solid wastes and also recover the energy contained in wastes [4, 5]. Combustion reduces the volume of wastes by about 90 % and its weight by 75 %, and the global WTE industry generates about 45 billion kWh of electricity. An equal amount of thermal energy for district heating and industrial use is also produced by the global WTE industry [4]. However, combustion of 100 % biomass causes severe corrosion problems since wastes often contain contaminants such as chlorides, sulfur and heavy metals [5, 6].

Boiler corrosion constitutes a significant problem in WTE plants, causing significant wall thinning of super-heater tubes, frequent shut-downs for maintenance, and high operational costs [3, 5, 7–10]. The conventional boilers are designed with high steam conditions ranging from 450 to 540℃ [1]. However, the super-heater steam temperature of major WTE boilers is limited to < 450℃ due to corrosion [11]. A corrosion rate of 40.6 mm/yr was reported in carbon steel super-heaters of a German incinerator [12]. Experience from Swedish power stations fired with 100 % wood-based biofuels has shown that conventional super-heater steels (low-chromium ferritic steels) have to be replaced after about 20,000 h if the steam temperature is 470°C or higher

[13]. Even for high-nickel, high-molybdenum alloys, such as alloy 625, significant wall thinning of super-heater tubes due to fireside corrosion can take place [14]. In a demonstration test completed at a WTE plant in Japan which generated steam of 500°C, the corrosion rate of alloy 625 super-heater tubes was estimated to be 1.91 mm/13,800 h in one section and 3.00 mm/13,800 h at the soot blower-affected zone [11]. Several studies have been reported and reviewed regarding corrosion in WTE boilers [5, 14–16]. It is generally agreed that chemical attack caused by deposits formed on boiler tube walls is considered to be the primary cause of corrosion in WTE plants. As the hot combustion gases flow over the heat transfer surfaces, both chloride and sulfate containing ashes deposit on the tubes and promote high-temperature corrosion [14]. A high corrosion rate occurs especially when the deposit is melted [2, 17]. As well, it is generally agreed that the main chemical elements involved in boiler corrosion are Cl, S, alkali metals (Na and K), and heavy metals (Pb, Zn and Ca) [18–20].

The electrical efficiency of a WTE plant was reported to be ~25 % with steam temperature of 420°C [21] compared to a coal-fired plant at ~47 % with steam temperature of 580°C [3]. It is known that the corrosion environment of WTE plants can be extremely aggressive upon raising the steam temperature above 500°C even for corrosion-resistant superalloys [11, 14]. However, customers of WTE plants are demanding increased thermal performance to achieve a higher electrical efficiency and thus the temperature of super-heater alloy surfaces could exceed those for which reliable corrosion information exists. On the other hand, it is not necessarily an option to change the nature of the feed materials. Therefore, increased thermal performance

requires the evaluation of the corrosion resistance of candidate alloys. Candidate alloys evaluated in this work range from low-chromium ferritic steels to nickel-based superalloys. Even though the deposits in boilers are always mixtures of different salts, a better understanding of the effects of single salts on the corrosion behavior of candidate alloys is required. Hence, in this work, the corrosiveness of various metal chlorides/sulfates, including KCl, NaCl, $PbCl_2$, $ZnCl_2$, $FeCl_2$, $CaCl_2$, $PbSO_4$, and $ZnSO_4$, was evaluated and compared on boiler tube materials (T22, 310H, Inconel 625, 347H, Esshete 1250, and Sanicro 28) at 500°C. In addition, a kinetic study on the hot corrosion of T22, Esshete 1250, and Sanicro 28 was carried out under simulated WTE ashes at 500°C for 1000 h.

2 Experimental Procedures

2.1 Materials and Experimental Set-Up

The chemical composition and densities $\left(\rho, \frac{g}{cm^3}\right)$ of the investigated boiler tube materials are presented in Table 1. Samples of 347H, 310H, and Inconel 625 were rectangular (1 cm x 1 cm x 1.5 cm) with a total surface area of 8 cm^2, and samples of T22 (3.8 cm OD x 2.4 cm ID x 0.8 cm Length), Esshete 1250 (3.7 cm OD x 2.7 cm ID x 1.0 cm Length), and Sanicro 28 (4.2 cm OD x 2.9 cm ID x 0.7 cm Length) were quarter pieces (90° portions) cut from boiler tubes with a total surface area of 8.45 cm^2. The salts used were KCl, NaCl, $CaCl_2$, $FeCl_2$, $ZnCl_2$, $PbCl_2$, $ZnSO_4$, $PbSO_4$, and one mixed salt (named Mixture A). Mixture A is a mixed salt prepared to simulate super-heater deposits. The chemical composition of Mixture A (2.1 wt% NaCl, 5.6 wt% Na_2SO_4, 2.6 wt% KCl, 41.8 wt% K_2SO_4, 5.0 wt% $PbCl_2$, 6.0 wt% $PbSO_4$, 6.0 wt% PbO, 2.4 wt% $ZnCl_2$, 5.2 wt%

$ZnSO_4$, 4.1 wt% ZnO, Bal. SiO_2) was determined according to the typical concentration ranges of the main corrosion-related elements (Cl, S, Na, K, Pb and Zn) in deposits from WTE plants [2, 22, 23]. Figure 1 presents the sketch of the hot corrosion setup. As shown in Fig. 1, the test specimens were embedded in a salt bath with approximately 5 g of each salt. There was some air left in the crucible.

Table 1. Chemical composition and densities of the investigated boiler tube materials (wt%)

Alloys	ρ, g/cm^3	Chemical Composition					
		Fe	Ni	Cr	Mo	C	Others
T22	7.76	Bal.	-	2	1	0.15	-
Esshete 1250	7.90	Bal.	9.5	15	1	0.1	1 Nb, 6.3 Mn
Sanicro 28	8.00	Bal.	31	27	3.5	0.02	2 Mn
SS310H	7.89	Bal.	21	25	-	0.08	-
SS347H	7.96	Bal.	11	18	-	0.08	1 Nb + Ta, 2 Mn
Inconel 625	8.44	5	Bal.	22	9	-	3.65 Nb + Ta

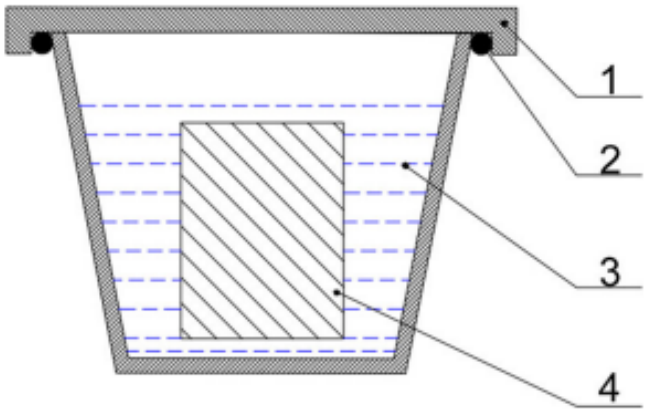

Figure 1. Sketch of hot corrosion setup. *1*, Crucible with cover; *2*, High-temperature sealant; *3*, Salts; *4*, Testing sample

Before the experiments, samples were ground with 600-grit SiC papers, cleaned in an ultrasonic bath with acetone, and weighed (recorded as the original weight, W_o). Then samples were placed in empty crucibles and preheated at 500°C for 24 h. After this pre-oxidation stage, salts were placed on the samples. In order to prevent salt vaporization and contamination, the crucibles, with an inner volume of 15 mL, were covered and sealed with high-temperature sealant (High-Temperature Gasketing Adhesive, McMaster-CARR). Sealed crucibles with single salts were left in the furnace at 500°C for 500 h. In the case of Mixture A, sealed crucibles were left in the furnace at 500°C for 250, 500, and 1000 h, respectively. There were duplicates for every condition, and data presented in this work are the mean values.

2.2 Post-exposure Procedures and Degradation Assessment

After hot crucible immersion testing, the high-temperature sealant was not damaged. Therefore, the system can be understood to be a closed system. Each sealed crucible was cooled in the furnace to room temperature, placed in a sealed plastic bag, and then stored in sealed desiccators. The crucibles were then disassembled carefully to retrieve the samples. After each step, the samples were immediately put into sealed desiccators to avoid moisture accumulation.

For samples from single salts, the extent of corrosion damage was determined by the mass-loss data together with the remaining oxide layer thicknesses of coupons after 500 h of exposure. The corrosion products were removed from samples by pickling with a basic potassium permanganate solution (2.5 M NaOH, 0.2 M $KMnO_4$) for 20 min at

80°C [2, 17]. Samples were then cleaned with acetone for 5 min in an ultrasonic bath and weighed (recorded as the final weight, W_f). After these measurements, the samples were embedded in epoxy, and the cross section of the epoxied samples was polished to 1 μm. Samples from single salts were analyzed by Scanning Electron Microscopy (SEM).

On the other hand, for samples from Mixture A, the corrosion extent was only determined by measuring the thicknesses of the corrosion layers after exposure. Neither chemical treatment nor weighing was performed on samples from Mixture A. Samples from Mixture A were directly embedded into epoxy, polished to 1 μm, and analyzed by SEM with Energy-Dispersive X-Ray Spectroscopy (EDX).

3 Results and Discussion

3.1 Effects of Single Chlorides

In waste-fired boilers, metal and alkali chlorides deposited on the tubes can promote high-temperature corrosion. In this section, the corrosivity of six different chlorides (KCl, NaCl, $CaCl_2$, $FeCl_2$, $ZnCl_2$ and $PbCl_2$) was evaluated and compared for different boiler tube materials (T22, 310H, Inconel 625, 347H, Esshete 1250, and Sanicro 28) at 500°C. After 500 h of exposure, it was noticed that severe corrosion and peeling-off of corrosion layers occurred on most of the samples exposed to $FeCl_2$, $ZnCl_2$ and $PbCl_2$. Therefore, mass-loss data together with remaining oxide layer thicknesses of coupons after 500 h of exposure were used in order to investigate the corrosion damage and associated mechanisms. The normalized mass loss (ΔM_N, g/cm^2) was calculated by Equation (i):

$$\Delta M_N = \frac{W_o - W_f}{A}, \quad \text{(i)}$$

where W_f (g) is the final weight, W_o (g) is the initial weight, and A (cm^2) is the surface area of the coupons.

Figure 2 shows the mass-loss data of boiler tube materials after 500 h of exposure. Negative values in Fig. 2 represent the mass-gain data after 24 h of pre-oxidation, which indicates the formation of oxide scales formed on samples. For the studied boiler tube materials, the mass-loss data indicate a general increasing trend of corrosivity in the order $CaCl_2$ (Melting Temperature, T_m = 772°C) < NaCl (T_m = 801°C) < KCl (T_m = 770°C) < $ZnCl_2$ (T_m = 318°C) < $PbCl_2$ (T_m = 501°C) < $FeCl_2$ (T_m = 677°C). It has been reported that $ZnCl_2$ and $PbCl_2$ start to volatilize at around 327°C [24]. When volatilized chlorides react with steels at metal temperatures above 450°C, the protective oxides will be degraded and Cl_2(g) will be released through reactions (1)–(3) [2, 14]. Since the votatilization rates of metal chlorides at 500°C increase in the order NaCl < KCl < $ZnCl_2$ < $PbCl_2$ [24], it is reasonable that the corrosivity of these four chlorides follows the same trend. On the other hand, $CaCl_2$ can degrade the protective oxides through reactions (4–5) [25]. Because of the rapid thermal decomposition of $CaCl_2$ (reaction (4)) and the poor mobility of CaO, $CaCl_2$ does not have the opportunity to react extensively with the oxides as is the case for NaCl and KCl [25]. Therefore, $CaCl_2$ is less corrosive as compared to NaCl and KCl, and the same conclusion has been reported by Karlsson et al. [25].

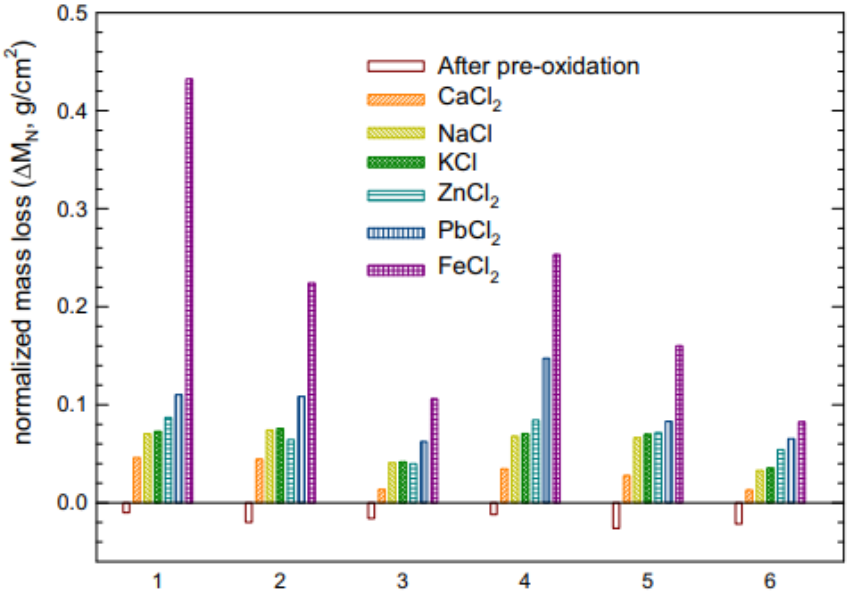

Figure 2. Mass-loss data of boiler tube materials after 500 h exposures in metal chlorides at 500°C. Negative values represent the mass-gain data after 24 h of pre-oxidation. 1 = T22; 2 = Esshete 1250; 3 = Sanicro 28; 4 = 347H; 5 = 310H; 6 = Inconel 625

For heavy metal chlorides,

$$Fe_2O_3 + 6\ Cl^-(PbCl_2, ZnCl_2) \rightarrow 2FeCl_3 + 3\ O^{2-}(PbCl_2, ZnCl_2), \quad (1)$$

$$2\ FeCl_3 + 1.5\ O_2(g) \rightarrow Fe_2O_3 + 3Cl_2(g) \quad (2)$$

For alkali chlorides,

$$2(Na,\ K)Cl + Fe_2O_3 + 0.5O_{2(g)} \rightarrow \ (Na,\ K)_2Fe_2O_4 + Cl_{2(g)}, \quad (3)$$

$$2CaCl_2 + O_{2(g)} \rightarrow 2CaO + 2Cl_{2(g)}, \quad (4)$$

$$2CaO + Fe_2O_3 + 1.5O_{2(g)} \rightarrow 2CaFeO_4. \quad (5)$$

In the proposed mechanism, first, the interaction of metal chlorides with metal oxide scales leads to the release of chlorine gas through reactions (1–4) and the formation of less-protective oxide scales (i.e., the degradation of metal oxides); then chlorine gas can penetrate through the less-protective metal oxide scale to the oxide/metal interface and react with iron or other metal components (such as Cr and Ni) to form volatile metal chlorides through reaction (6) [14]:

$$Fe + Cl_2 \rightarrow FeCl_2, \quad (6)$$

$$2FeCl_2 + 1.5O_2 \rightarrow Fe_2O_3 + 2Cl_2, \quad (7)$$

$$3FeCl_2 + 2O_2 \rightarrow Fe_3O_4 + 3Cl_2. \quad (8)$$

Then volatile metal chlorides diffuse outward through the scales covering the metal surface and react with oxygen to form metal oxides and chlorine [14]. The above reactions are eventually trapped in a vicious cycle: reaction (7/8) → reaction (6) → reaction (7/8). Therefore, the reaction sequences for the studied metal chlorides can be described as follows:

For $ZnCl_2$/$PbCl_2$: reaction (1) → reaction (2) → reaction (6) → reaction (7/8) → reaction (6) → reaction (7/8);

For NaCl/KCl: reaction (3) → reaction (6) → reaction (7/8) → reaction (6) → reaction (7/8);

For $CaCl_2$: reaction (4) → reaction (6) → reaction (7/8) → reaction (6) → reaction (7/8);

For $FeCl_2$: reaction (7/8) → reaction (6) → reaction (7/8).

In the case of $FeCl_2$, metals corrode directly through the vicious cycle of reaction (7/8)

→ reaction (6) → reaction (7/8), which is shorter than the reaction sequences of the other studied metal chlorides. Further, the corrosion rates of metals in the above metal chlorides, with the exception of $FeCl_2$, also depend on the kinetics of these reactions, which occur before the vicious cycle of reaction (7/8) → reaction (6) → reaction (7/8). Therefore, it is understandable that $FeCl_2$ is the most corrosive salt among all single chlorides studied in this work. The above discussion supports the conclusion made based on Fig. 2: the corrosivity of the studied metal chlorides increases in the order $CaCl_2$ < NaCl < KCl < $ZnCl_2$ < $PbCl_2$ < $FeCl_2$.

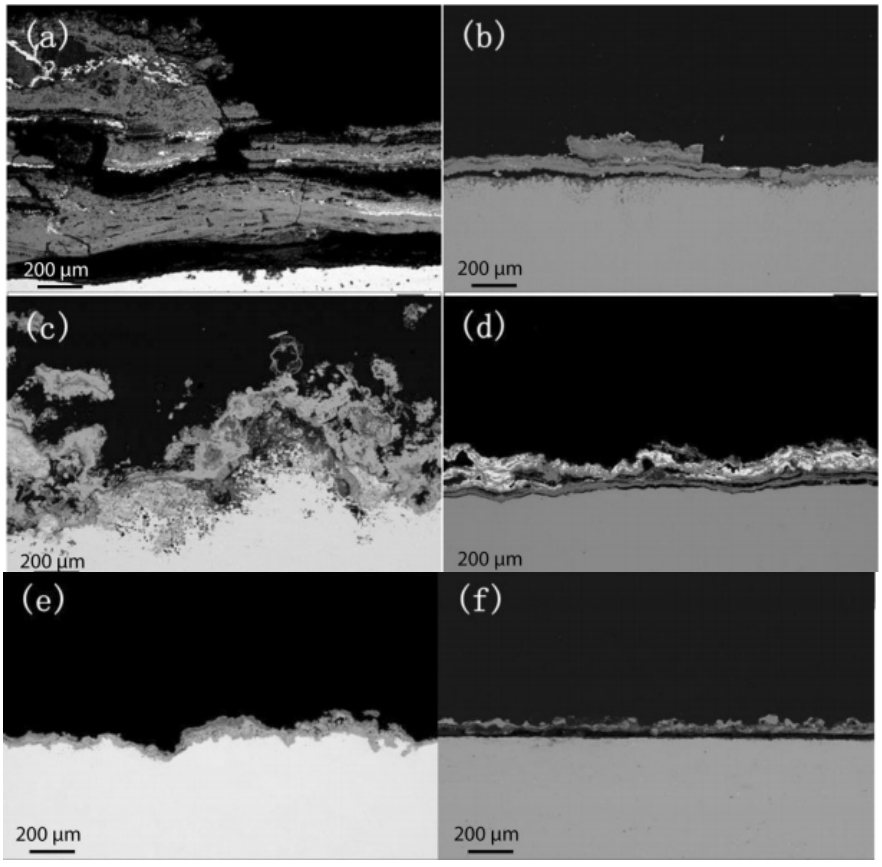

Figure 3. Cross-section SEM images of **a** T22, **b** 347H, **c** Esshete 1250, **d** 310H, **e** Sanicro 28, and **f** Inconel 625 samples after 500 h exposures in $PbCl_2$ at 500°C

Cross-section SEM images were taken on coupons after 500 h of exposure in single chlorides. An example is presented in Fig. 3. The corrosion layer morphologies of candidate alloys can be divided into two groups: uniform corrosion for T22, 310H, and Inconel 625, and uniform corrosion with grain boundary degradation/pitting corrosion for 347H, Esshete 1250, and Sanicro 28. It is worth mentioning that grain boundary degradation has been observed on Esshete 1250 in mixed alkali salts at 500°C [16], and 347H and Sanicro 28 in alkali chlorides at 475–650°C [26]. The internal degradation of these alloys has been partially explained by their large grain sizes, which can slow down the formation/healing of the protective chromium oxide [26]. As well, the rapid reaction of chloride vapor and oxygen with metal and metal oxides is used to interpret the internal degradation by chloride salts, especially at grain boundaries at high temperatures [27].

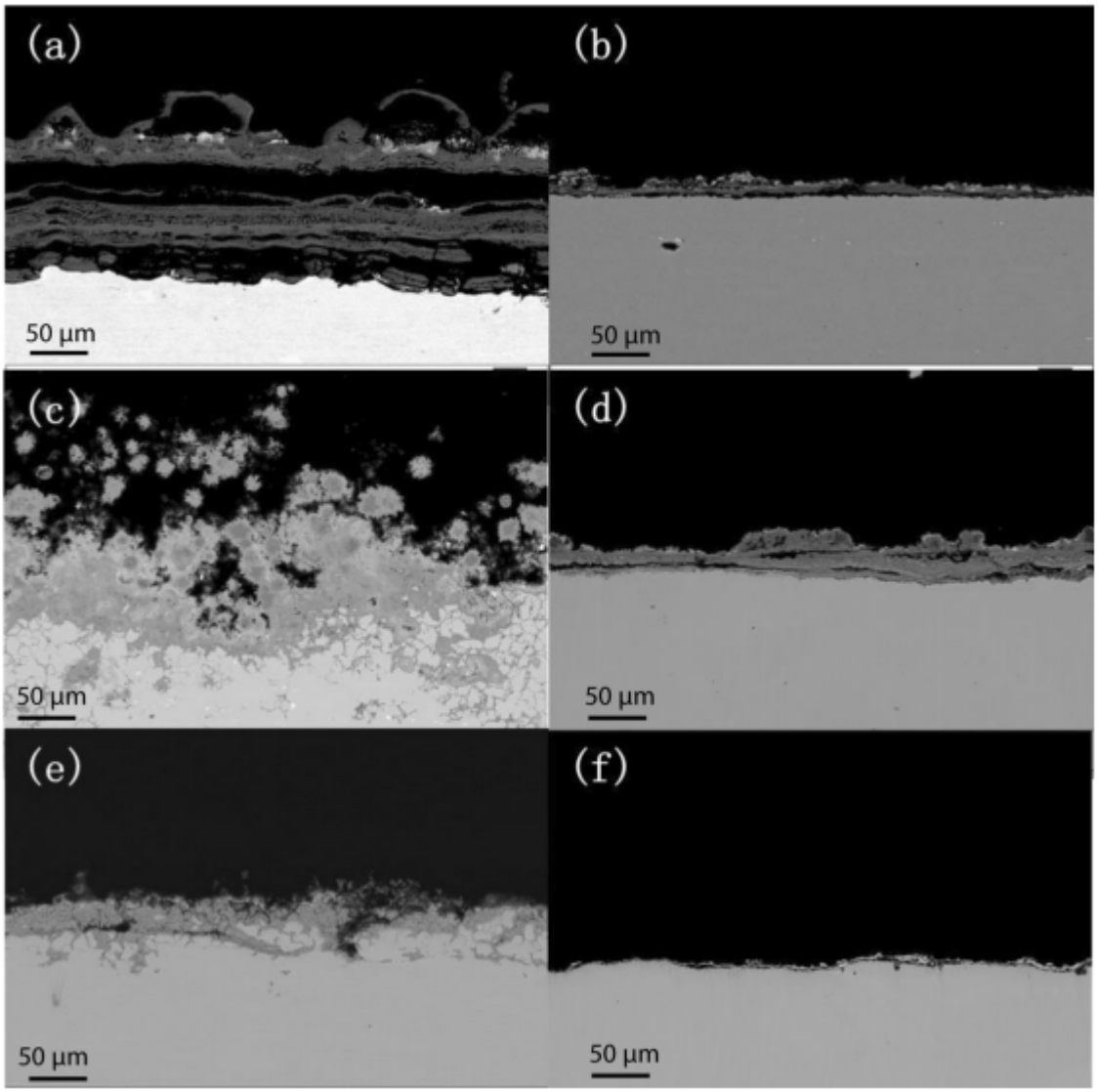

Figure 4. Cross-section SEM images of **a** T22, **b** 347H, **c** Esshete 1250, **d** 310H, **e** Sanicro 28, and **f** Inconel 625 samples after 500 h exposures in $PbSO_4$ at 500°C

3.2 Effects of Zn- and Pb-Containing Salts

In recovered waste wood, main surface treatments, such as white pigment (zinc and lead oxides) in paints, contribute to an increase in the amounts of Zn and Pb. Moreover, Pb- and Zn containing compounds are widely used in polyvinyl chloride (PVC) as metal stabilizers [28]. Zn and Pb may react with S and Cl to form chlorides and sulfates upon

combustion, and then deposit on boiler tubes. In the above section, it has been proven that Zn and Pb chlorides can cause severe corrosion of boiler tube materials. In order to study the hot corrosion of boiler tube materials in the Zn- and Pb-rich environments, the corrosivity of $ZnSO_4$ and $PbSO_4$ was also investigated on different boiler tube materials at 500°C following the same experimental and analysis procedures as in the above section. In order to differentiate from Figs. 3, 4 shows the cross-section SEM images of boiler tube materials after 500 h of exposure in $PbSO_4$ salts. SEM images in Figs. 3 and 4 clearly demonstrate that, for the same alloy, the thickness of the corrosion layer from sulfate deposits is much thinner than that from chloride deposits. In addition, grain boundary degradation was observed on 347H, Esshete 1250, and Sanicro 28 coupons after 500 h of exposure in Zn and Pb sulfates at 500°C.

Generally, the degradation thicknesses (calculated degradation thickness $\mathrm{d_c}$, cm) of uniformly corroded samples can be calculated from the mass-loss data, where $\mathrm{d_c}$ is equal to $\frac{\Delta \mathrm{M_N}}{\rho}$. Since coupons of 347H, Esshete 1250, and Sanicro 28 suffered from grain boundary degradation/pitting corrosion, it is not sufficient to use the calculated degradation thicknesses to quantify the degradation of these alloys. Therefore, the thickness of the corrosion layers (measured degradation thickness d_m, cm) on metals after removal of the corrosion products by chemical etching were collected through cross-section SEM images to provide further evaluation criteria. According to Bankiewicz's work, the thickness of the corrosion layer is defined as the outer corrosion product layer plus the internal oxidation and localized corrosion [19]. Figure 5 presents a typical cross-section SEM image and the principle of the thickness measurements for each corrosion layer, that is, d_m = A (outer corrosion products) + B (internal

oxide/localized corrosion). Figure 6 presents the total degradation thicknesses ($d_{total} = d_m + d_c, cm$) of all coupons in Zn- and Pb- containing salts. Results obtained after 500 h of exposure at 500°C suggest that T22 and Esshete 1250 present the worst corrosion resistance to Zn- and Pb-containing salts, while Inconel 625 presents the best corrosion resistance among the studied boiler tube materials.

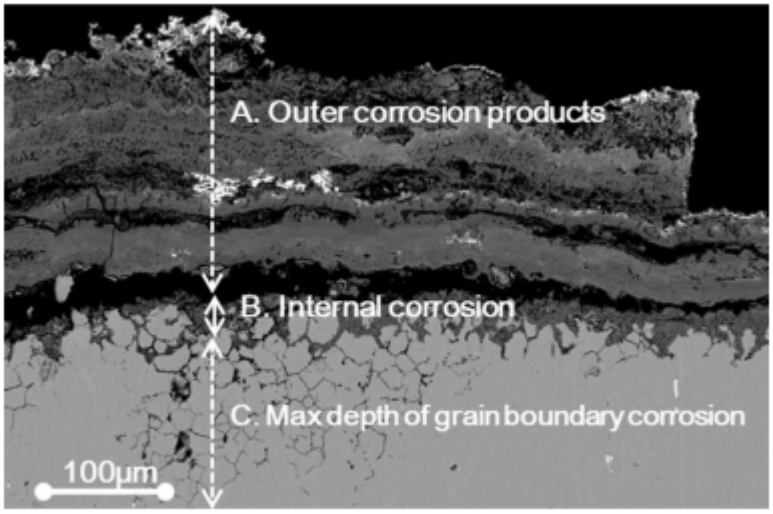

Figure 5. A typical cross-section SEM image and the principle of the thickness measurements for each corrosion layer. The 347H sample after 500 h of exposure in $PbCl_2$ at 500°C

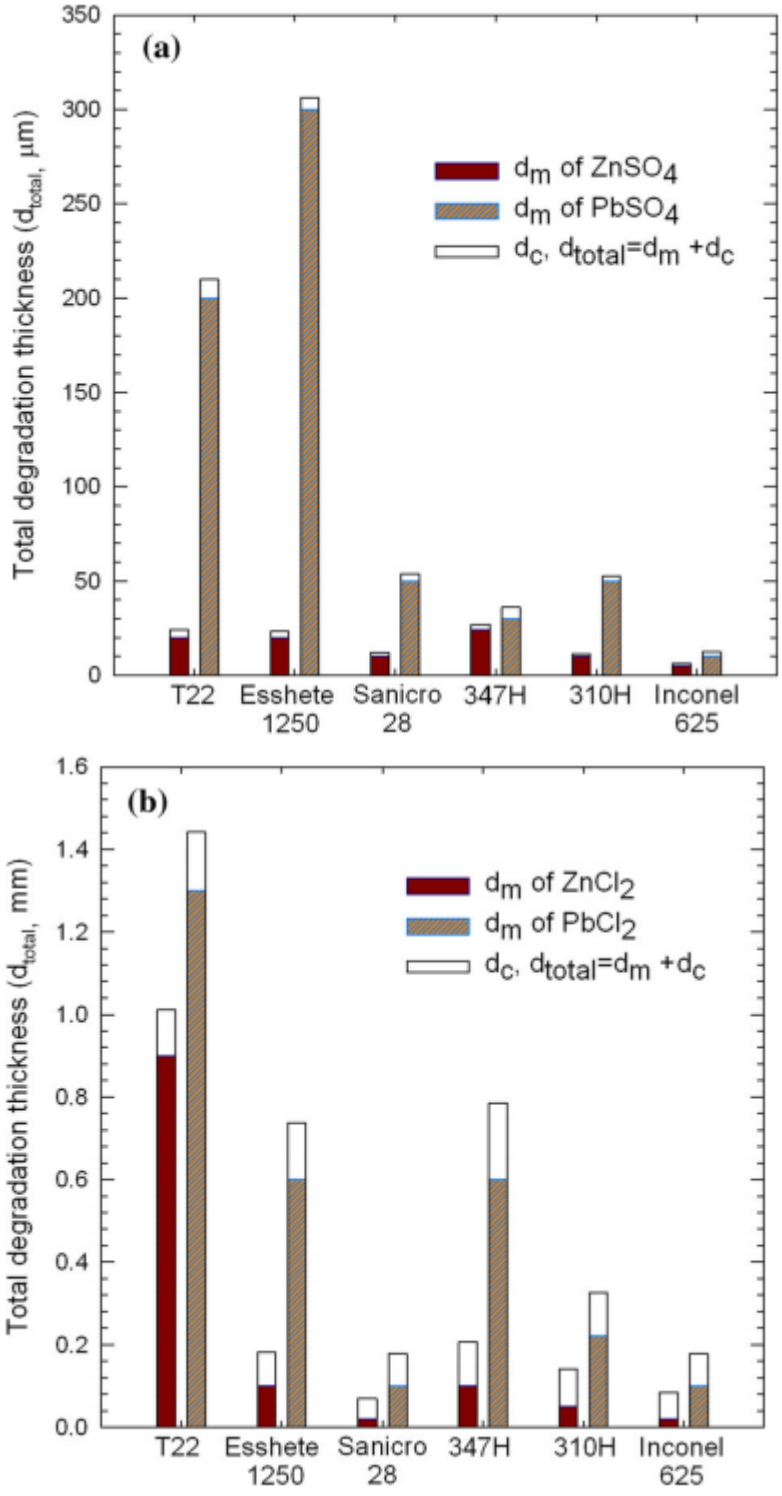

Figure 6. Total degradation thicknesses ($d_{total} = d_m + d_c$) of all coupons after 500 h exposures in **a** Zn and Pb sulfates, and **b** Zn and Pb chlorides at 500°C

As shown in Fig. 6, the degradation extents of candidate alloys in sulfates are all in the several tenth μm level; in comparison, their degradation extents in chlorides are much higher, in the mm level. It can be concluded that the sulfates of Zn and Pb are less corrosive than their chlorides. However, Zn, Pb, S, and Cl are all volatile elements [3]. The vaporization of material proceeds when its vapor pressure is lower than the saturated value [29]. According to previous evaporation investigations, Zn and Pb exist primarily as chlorides rather than sulfates in the vapor phase because of a higher saturated vapor pressures [30–32]. Mixtures containing Zn and Pb chlorides then will form melts at waterwall/super-heater temperatures in the presence of Cl [33]. Therefore, the presence of Zn and Pb has a strong influence on the degradation rates of boiler tubes as long as Cl exists in waste-fired boilers.

3.3 Hot Corrosion of Boiler Tube Materials Under Simulated WTE Ashes

Regardless of the various T_m values of the different metal chlorides, mixtures formed by metal chlorides may have Tm values below 500°C, such as 55$ZnCl_2$-45KCl ([mole %], T_m = 230°C), 28NaCl-56KCl-16$PbCl_2$ (T_m = 400°C), and 49NaCl-51$CaCl_2$ (T_m = 500°C) [2, 3, 34]. A few studies have reported the typical concentration ranges of the main corrosion-related elements (Cl, S, Na, K, Pb, and Zn) in deposits from WTE plants [2, 22, 23]. A mixture (Mixture A) was prepared to simulate the super-heater deposits, which contained the average level of corrosion-related elements (5.1 wt% Cl, 10.2 wt% S, 2.6 wt% Na, 20.4 wt% K, 13.5 wt% Pb, and 5.8 wt% Zn) reported in previous studies [2, 22, 23]. A kinetic study was then performed to simulate the hot corrosion of boiler tube materials under WTE ashes.

The influence of exposure time on the hot corrosion of boiler tube materials (T22, Esshete 1250, and Sanicro 28, which have the same geometry) in Mixture A at 500°C was tracked for an exposure time of 1000 h. As shown in Fig. 7, these three alloys exhibited comparable performance in the short term (250 h exposure). However, after the 1000 h exposure, the degradation thickness presented a clear tendency, decreasing in the order T22 > Esshete 1250 > Sanicro 28. Therefore, in terms of corrosion resistance, T22 and Sanicro 28 presented the worst and best performance, respectively. The degradation percentage (%) is calculated by Equation (ii):

$$\text{Degradation percentage } (\%) = \frac{\text{Degradation thickness after } x - \text{hours exposure}}{\text{Degradation thickness after } 1000 - \text{hours exposure}} \times 100\% \quad \text{(ii)}$$

As shown in the embedded figure of Fig. 7, 44, 59, and 70 % of the total degradation seen for the 1000 h exposure occurred on T22, Esshete 1250, and Sanicro 28 in the first 250 h, respectively; afterward, all alloys continued corroding but with different rates, T22 > Esshete 1250 > Sanicro 28. The difference in the corrosion kinetics of these three alloys can be explained by the Cr and Ni contents (T22, Esshete 1250, and Sanicro 28 are a low-alloy steel, austenitic stainless steel, and high-alloy austenitic stainless steel, respectively [19]).

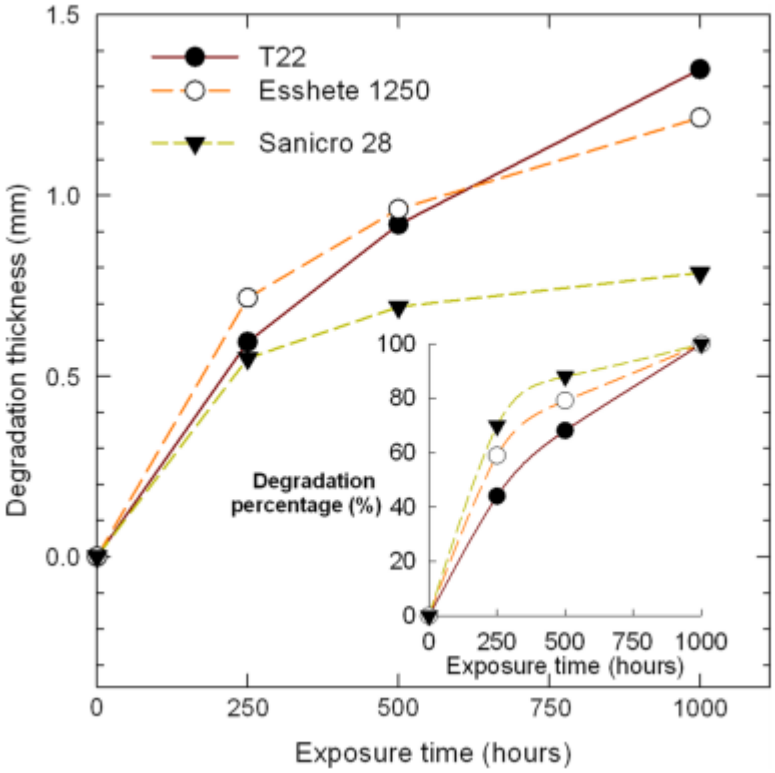

Figure 7. The influence of exposure time on the corrosion of T22, Esshete 1250, and Sanicro 28 in simulated super-heater deposits (Mixture A) at 500°C

Cr and Ni are important for the formation of protective oxides on steels, and their beneficial effect in retarding corrosion in WTE systems has been reported [1, 19]. Figure 8 presents the cross-sectional backscatter SEM images combined with elemental X-ray (EDX) maps. The EDX maps demonstrate that the oxide layer structures directly on top of the un-oxidized steels are a mixed Fe–Cr oxide layer for T22 in Fig. 8a, a thin Ni-rich layer followed by a mixed Fe–Cr oxide layer for Esshete 1250 in Fig. 8b, and a thicker Ni-rich oxide layer (compared to Fig. 8b) followed by a top layer of mixed oxides for Sanicro 28 in Fig. 8c. The EDX maps clearly reveal the role of Ni/Cr for slowing the corrosion kinetics of the studied alloys. That is, the Ni/Cr-rich oxide layer formed between the outer corrosion products and un-oxidized steels protected steels from

further corrosion attack.

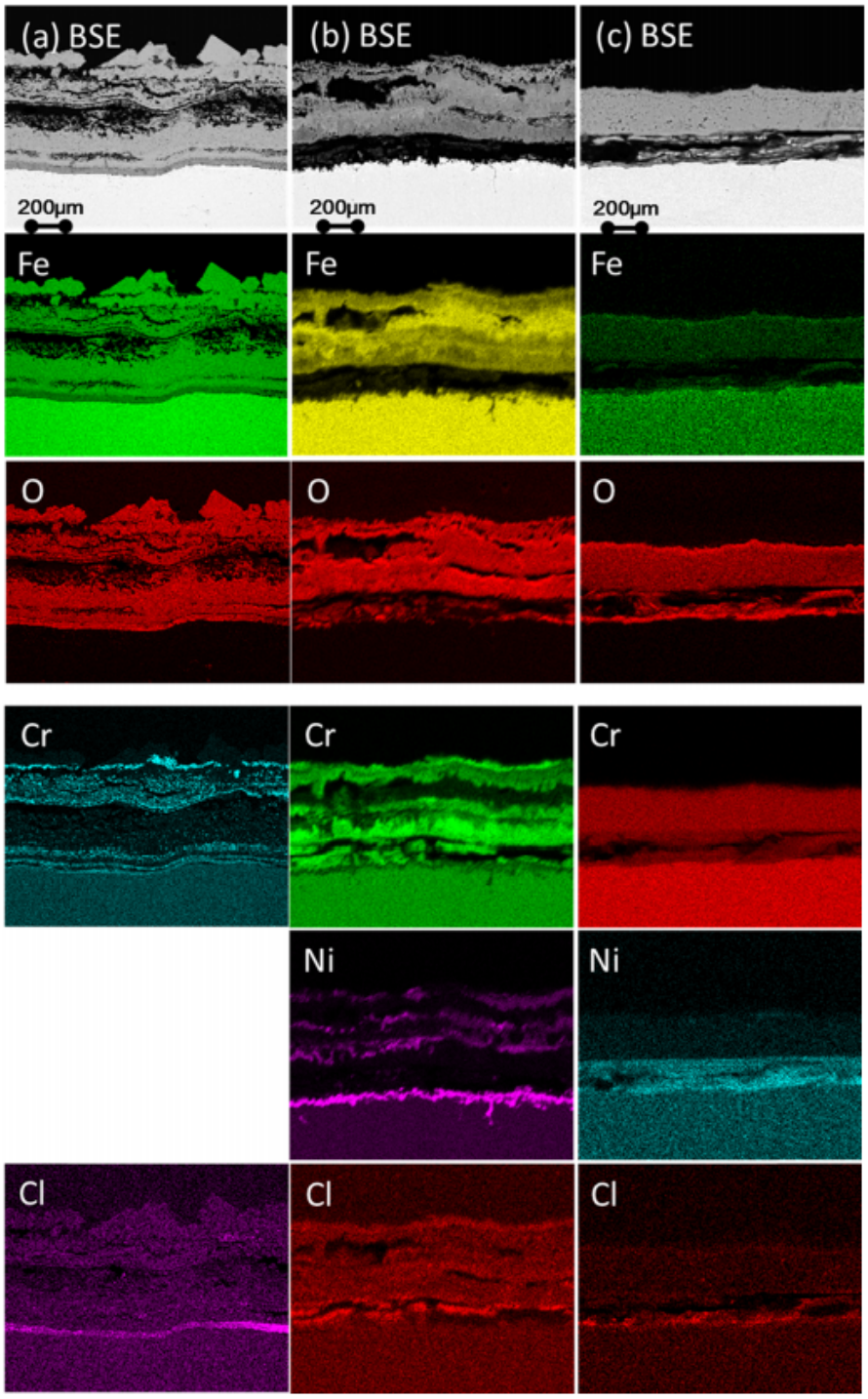

Figure 8. SEM/EDX maps of cross-section area of **a** T22, **b** Esshete 1250, and **c** Sanicro 28 after the 1000-h exposure in Mixture A at 500°C

4 Conclusions

Chlorides and sulfates in the ash deposits are known to be the main corrosive agents. In this work, the hot corrosion behavior of boiler tube materials (T22, 310H, Inconel 625, 347H, Esshete 1250, and Sanicro 28) was evaluated in WTE related environments at 500°C. Based on the experimental results, the following conclusions were obtained:

1. For the studied boiler tube materials, the mass-loss data indicate a general increasing trend of corrosivity as $CaCl_2$ < NaCl < KCl < $ZnCl_2$ < $PbCl_2$ < $FeCl_2$. Mechanisms to explain the different impacts of chlorides are proposed. It is believed that materials exposed to chloride salts corrode through vicious cycles in which a shorter path of the cycle leads to a higher corrosion rate. Experimental results confirmed that $FeCl_2$ with the shortest path of the corresponding vicious cycle has the highest corrosion rate. During the exposure in metal chlorides, 347H, Esshete 1250, and Sanicro 28 suffered from grain boundary degradation.
2. The sulfates of Zn and Pb are less corrosive than their chlorides. Due to their volatile ability, the presence of Zn and Pb still have a strong influence on the degradation rates of boiler tubes as long as Cl exists in waste-fired boilers. Results obtained after 500 h exposures at 500°C suggest that T22 and Esshete 1250 present the worst corrosion resistance to Zn- and Pb-containing salts, while Inconel 625 presents the best corrosion resistance among the studied boiler tube materials.
3. Results from the kinetic study show that T22, Esshete 1250, and Sanicro 28 exhibited comparable performance in a short-term exposure under simulated WTE ashes. However, the degradation thickness presented a clear tendency

after the 1000 h exposure, decreasing as T22 > Esshete 1250 > Sanicro 28. EDX maps clearly reveal the role of Ni/Cr for slowing the corrosion kinetics of these three alloys.

Acknowledgements

The authors gratefully acknowledge the financial support of the Natural Sciences and Engineering Research Council of Canada and Nexterra Systems Corporation.

References

1. G. Sorell, Materials at High Temperatures 14, 207 (1997).

2. M. Spiegel, Materials and Corrosion 50, 373 (1999).

3. M. Bøjer, P. A. Jensen, F. Frandsen, K. Dam-Johansen, O. H. Madsen and K. Lundtorp, Fuel Processing Technology 89, 528 (2008).

4. Y.-H. Chang, W. Chen and N. B. Chang, Journal of Hazardous Materials 58, 33 (1998).

5. D. Mudgal, S. Singh, S. Prakash, International Journal of Corrosion (2014).

6. M. Becidan, L. Sørum, F. Frandsen and A. J. Pedersen, Fuel 88, 595 (2009).

7. S. Kamal, R. Jayaganthan, S. Prakash and S. Kumar, Journal of Alloys and Compounds 463, 358 (2008).

8. R. A. Mahesh, R. Jayaganthan and S. Prakash, Journal of Alloys and Compounds 460, 220 (2008).

9. S. H. Cho, J. M. Hur, C. S. Seo, J. S. Yoon and S. W. Park, Journal of Alloys and Compounds 468, 263 (2009).

10. S. H. Cho, J. M. Hur, C. S. Seo and S. W. Park, Journal of Alloys and Compounds 452, 11 (2008).

11. N. Otsuka, Corrosion Science 50, 1627 (2008).

12. H. Krause, Historical perspective of fireside corrosion problems in refuse-fired boilers, Paper No. 93200, Corrosion/93, NACE International, (1993).

13. P. Henderson, P. Ljung, P. Kallner, J. Tollin, Fireside corrosion of superheater materials in a wood-fired circulating fluidised bed boiler, EUROCORR 2000 conference, September 10-14, 2000, London, published Institute of Materials, Minerals and Mining,

London, 2000.

14. S. H. Lee, N. J. Themelis and M. J. Castaldi, Journal of Thermal Spray Technology 16, 104 (2007).

15. B. J. Skrifvars, R. Backman, M. Hupa, K. Salmenoja and E. Vakkilainen, Corrosion Science 50, 1274 (2008).

16. B. J. Skrifvars, M. Weste´n-Karlsson, M. Hupa and K. Salmenoja, Corrosion Science 52, 1011 (2010).

17. M. Sa´nchez and M. Paste´n, Materials and Corrosion 57, 192 (2006).

18. C. Chan, C. Q. Jia, J. W. Graydon and D. W. Kirk, Journal of Hazardous Materials 50, 1 (1996).

19. D. Bankiewicz, Corrosion behaviour of boiler tube materials during combustion of fuels containing Zn and Pb, Academic Dissertation, A˚ bo Akademi, Faculty of Chemical Engineering, Process Chemistry Centre, A˚ bo (2012).

20. M. Norell, P. Andersson, Field test of waterwall corrosion in a CFB waste boiler, Paper No. 00236, Corrosion 2000, NACE International (2000).

21. P. Vainikka, S. Enestam, J. Silvennoinen, R. Taipale, P. Yrjas, A. Frantsi, J. Hannula and M. Hupa, Fuel 90, 1101 (2011).

22. M. Born, VGB Powertech 85, 107 (2005).

23. H. P. Nielsen, F. J. Frandsen and K. Dam-Johansen, Energy & Fuels 13, 1114 (1999).

24. S. Osada, D. Kuchar and H. Matsuda, Journal of Material Cycles and Waste Management 11, 367 (2009).

25. S. Karlsson, J. Pettersson, L. G. Johansson and J.-E. Svensson, Oxidation of

Metals 78, 83 (2012).

26. S. Enestam, D. Bankiewicz, J. Tuiremo, K. Ma¨kela¨ and M. Hupa, Fuel 104, 294 (2013).

27. H. Pickering, F. Beck and M. Fontana, Materials Transactions ASM 53, 793 (1961).

28. F. J. Frandsen, A. J. Pedersen, J. Hansen, O. H. Madsen, K. Lundtorp and L. Mortensen, Energy & Fuels 23, 3490 (2009).

29. Y. L. Zhang and E. Kasai, ISIJ International 44, 1457 (2004).

30. S. K. Durlak, P. Biswas and J. Shi, Journal of Hazardous Materials 56, 1 (1997).

31. S. Stucki and A. Jakob, Waste Management (Oxford) 17, 231 (1998).

32. G. Trouve, A. Kauffmann and L. Delfosse, Waste Management (Oxford) 18, 301 (1998).

33. I.G. Wright, H.H. Krause, Assessment of factors affecting boiler tube lifetime in waste-fired steam generators: new opportunities for research and technology development, Report No. NREL/TP–430-21480. National Renewable Energy Lab., Golden, CO (United States) (1996).

34. H. Krause, Corrosion by chlorine in waste-fueled boilers, R.W. Bryers (Ed.), Proceedings of the Incinerating Municipal and Industrial Waste—Fireside Problems and Prospect for Improvement Conference, Sheraton Palm Coast, Hemisphere Press (1989), p. 145.